Journal of Solid State Chemistry 184 (2011) 712–719

Contents lists available at ScienceDirect

Journal of Solid State Chemistry

journal homepage: www.elsevier.com/locate/jssc

Formation of titanate nanostructures under different NaOH concentration and their application in wastewater treatment

Jiquan Huang [a,b], Yongge Cao [a,*], Zhonghua Deng [a], Hao Tong [a]

[a] Key Lab of Optoelectronic Materials Chemistry and Physics, Fujian Institute of Research on the Structure of Matter, Chinese Academy of Sciences, Fuzhou 350002, China
[b] Graduate school of Chinese Academy of Sciences, Chinese Academy of Sciences, Beijing, 100049, China

ARTICLE INFO

Article history:
Received 17 September 2010
Received in revised form
24 December 2010
Accepted 17 January 2011
Available online 25 January 2011

Keywords:
Titanate nanostructure
NaOH concentration
Wastewater
Adsorption
Photocatalysis

ABSTRACT

The effects of the concentration of NaOH on the formation and transformation of various titanate nanostructures were studied. With increasing NaOH concentration, three different formation mechanisms were proposed. Nanotubes can only be obtained under moderate NaOH conditions, and should transform into nanowires with prolonged hydrothermal treatment, and their formation rate is accelerated by increasing NaOH concentration. Low concentration of NaOH results in the direct formation of nanowires, while extra high concentration of NaOH leads to the formation of amorphous nanoparticles. Adsorption and photocatalysis studies show that titanate nanowires and nanotubes might be potential adsorbents for the removal of both heavy metal ions and dyes and photocatalysts for the removal of dyes from wastewater.

1. Introduction

Since the discovery of nanotubular titanate produced by the hydrothermal treatment of titania with alkaline solution in 1998 [1], various titanate nanostructures, such as nanotubes, nanowires, nanoflowers and nanosheets, have been widely developed due to their riddling structures and attractive potential applications [2–11]. The unique physical and chemical properties of these materials make them highlighted in various applications, such as in catalysts [12], hydrogen storage [13,14], solar batteries [15,16], Li-ion batteries [17–19], electrochromism [20] and gas sensors [21]. It is found that the titanate nanostructures combine the properties of conventional titanate (e.g. ion exchange) and titania (e.g. photocatalysts) [22]. Additionally, the titanate nanostructures can be used as excellent adsorbents for the removal of both inorganic and organic pollutants, such as heavy metal ions and dyes, from wastewater [9,23,24], due to their flexible interlayer distances and high surface area. In other words, titanate nanostructures can be used as ion-exchangers, adsorbents and photocatalysts. This multi-role characteristic of titanate nanostructures enables them to have advantages in wastewater treatment. On the other hand, with regard to the envisaged and optimized applications of these titanate nanomaterials, it is necessary to clarify their structures, formation and transformation mechanisms, and thereby achieve perfect control of their morphology, surface area and crystallinity. However, up to date, the exact formation mechanisms and chemical compositions of the titanate nanostructures are still under disputation despite intensive investigations.

It is doubtless that the hydrothermal temperature, duration and the concentration of NaOH are three crucial parameters that affect the morphologies and structures of the products in the reaction. Up to now, most of the studies focused on the hydrothermal temperature or duration, and most of the experiments were carried out under the moderate alkali condition, typically 10 M NaOH solution. However, few attentions have been paid to the systemic study on the effects of NaOH concentration [25].

In this study, we present a detailed investigation on the effects of the concentration of NaOH on the structures and formation mechanisms of various titanate. It is found that the morphologies of the titanate products were determined by the reaction conditions, especially the concentration of NaOH. In this paper, we also report the removal of heavy metal ions and dyes from water system by using the as-prepared titanate nanotubes, nanowires and amorphous titanate nanoparticles as adsorbents and photocatalysts. It is hoped that our investigations would help to the further understanding of various titanate nanomaterials and accelerate the application process.

2. Experimental

2.1. Preparation of various titanate nanostructures

Various titanate nanostructures were synthesized by the hydrothermal process similar to that described by Kasuga et al. [1].

* Corresponding author. Tel: +86 591 83721039; Fax: +86 591 83713291.
E-mail address: caoyongge@fjirsm.ac.cn (Y. Cao).

0022-4596/$ - see front matter © 2011 Elsevier Inc. All rights reserved.
doi:10.1016/j.jssc.2011.01.023

Experiments were carried out as follows. 0.25 g of anatase TiO_2 nanopowder was added to 20 mL of NaOH aqueous solution with concentration of NaOH ranging from 2 to 20 M. After stirring for 0.5 h, the specimen was transferred into a 25 mL autoclave and then heated at 180 °C in an oven. The hydrothermal duration was varied from 0.5 to 360 h. After the hydrothermal reaction, the precipitate was collected and washed with distilled water and ethanol several times and then dried in air at 70 °C for 10 h. In order to convert nanostructured titanates into their protonated form, the powder was washed several times with 0.01 M HCl solution, followed by distilled water washing to pH 6 and then absolute ethanol for three times. Finally, the products were dried in air at 110 °C overnight.

2.2. Adsorption and photocatalysis studies

For the determination of the isotherms of metal ions adsorption, the protonated titanate adsorbent of amount 0.1 g was added into 100 mL of $Pb(NO_3)_2$ aqueous solutions with desired concentrations (from 3×10^{-5} to 6×10^{-3} M), followed by stirring for 2 h at room temperature. The adsorbents were then separated from the suspension via centrifugation and the concentration of metal ions in the supernate was detected by the Ultima2 ICP optical emission spectrometer.

For measurement of the dye adsorption isotherms, 0.1 g of the protonated titanate adsorbent was added into 100 mL of methylene blue solution with desired concentration (5×10^{-6} to 6×10^{-4} M), followed by stirring for 2 h at room temperature. The adsorbents were then separated from the suspension via centrifugation and the concentration of dye in the supernate was determined using a Perkin-Elmer Lambda 35 UV–visible spectrometer; absorption band at 665 nm was used.

The photocatalytic activity was evaluated by degradation of methylene blue. 0.1 g of the protonated titanates was added into 100 mL of methylene blue solution, and the initial concentration of the methylene blue solution (after stirring in the dark for 12 h) was 2×10^{-5} M. The suspension was irradiated under two 30 W low-pressure Hg lamps with a peak wavelength of 254 nm. The distance between the suspension and the UV lamp was 20 cm. At given intervals, 5 mL of the suspension was extracted and subsequently centrifuged. The concentration of dye in the supernate was determined using a Perkin-Elmer Lambda 35 UV–visible spectrometer.

2.3. Samples characterization

The morphologies and microstructures of the resultant products were observed by scanning electron microscopy (SEM) and transmission electron microscopy (TEM). The phase and crystal structure were analyzed by X-ray diffraction (XRD). The elemental analysis of the sample was conducted by energy-dispersive X-ray (EDX) spectroscopy on the scanning electron microscopy. The concentration of Ti(IV) in alkaline solution and the chemical compositions of various titanate nanostructures were determined by the Ultima2 ICP optical emission spectrometer.

3. Results and discussion

3.1. Effect of NaOH on the formation of titanate nanostructures

Fig. 1 shows the TEM images of the hydrothermal products obtained by treating TiO_2 in NaOH solution with different concentrations at 180 °C for 24 h. It was observed that under the different concentrations of NaOH (C_{NaOH}), i.e., 3, 5, 10, 12 and 15 M, the products were nanosheets, nanotubes, admixture of nanotubes and nanowires, nanowires and amorphous particles, respectively, as shown in Fig. 1a–e. The titanate nanotubes have lengths of several hundreds of nanometers and outer diameters of about 7–10 nm. The wall thickness of the nanotubes is about 2–4 nm, composed of 3–5 layers. The nanowires have widths ranging from 40 to 250 nm and lengths of several tens of micrometers. The corresponding XRD patterns of these hydrothermal products are displayed in Fig. 2. The XRD pattern of $H_2Ti_2O_5\cdot H_2O$ (JCPDS, Card no. 47-0124), which is identical to $H_2Ti_2O_4(OH)_2$ [26,27], is also shown at the bottom of Fig. 2. The observed diffraction peaks at $2\theta=9.8°$, 23.9°, 28.0°, 48.0° and 61.9° for both titanate nanosheets and nanotubes correspond well with those of lattice planes (200), (110), (310), (020) and (002) of

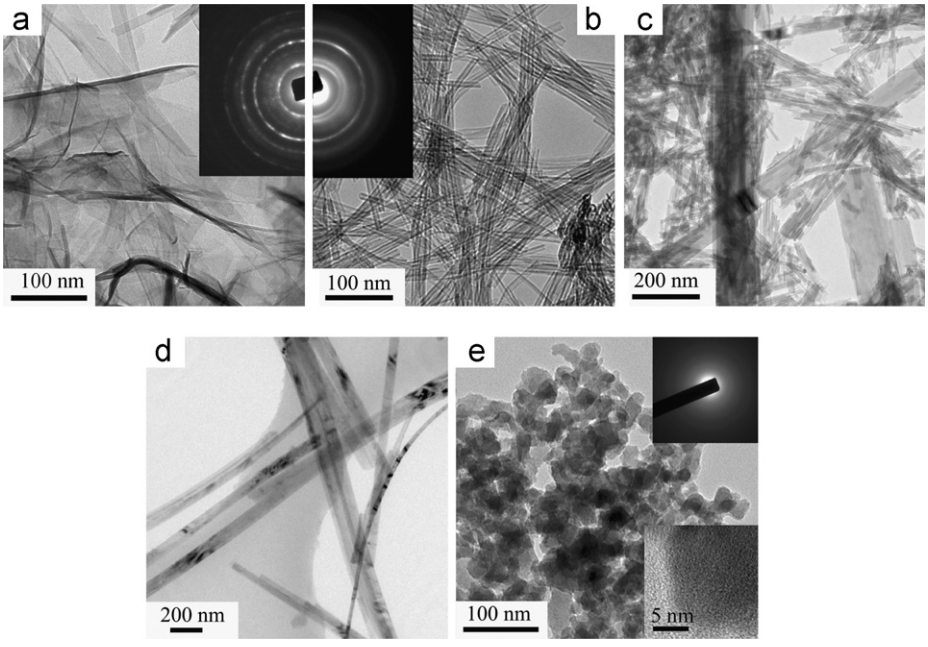

Fig. 1. TEM images of the hydrothermal products obtained by treating TiO_2 in NaOH solution with different NaOH concentration: (a) 3 M, (b) 5 M, (c) 10 M, (d) 12 M and (e) 15 M at 180 °C for 24 h. The insets (a, b) and (e) are corresponding SAED patterns and HRTEM image.

orthorhombic $H_2Ti_2O_5 \cdot H_2O$. The structure of the nanotubes (and nanosheets) is thus assumed as layered $Na_2Ti_2O_5 \cdot H_2O$ ($Na_2Ti_2O_4(OH)_2$), which is further supported by both ICP and EDX detection. ICP detection indicates that the Na/Ti mole ratio is about 1.05, 0.97 and 0.47 for nanosheets, nanotubes and nanowires, respectively. EDX measurement shows that the Na/Ti atomic ratio is about 0.89 and 0.48 for nanotubes and nanowires respectively. The Na/Ti mole ratio is very close to the theoretical ratio of 1 for both nanosheets and nanotubes. The XRD pattern of the nanowires is in remarkable agreement with that of the monoclinic $NaTi_2O_4(OH)$ [28], which is further demonstrated by the EDX and ICP detection, as mentioned above.

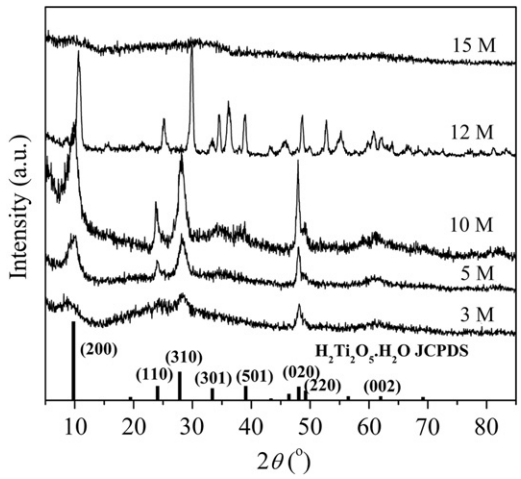

Fig. 2. XRD pattern of the hydrothermal products obtained by the treatment of TiO_2 in NaOH solution with different concentration at 180 °C for 24 h. The standard diffraction pattern of $H_2Ti_2O_5 \cdot H_2O$ from JCPDS (No. 47-0124) is provided at the bottom of this figure.

As shown in Fig. 1, lower alkaline condition (e.g., $C_{NaOH}=3$ M) results in the formation of nanosheets, while increasing of the NaOH concentration leads to the formation of nanotubes ($C_{NaOH}=5$ M, Fig. 1b) and even nanowires ($C_{NaOH}=12$ M, Fig. 1d). Similarly, it had been reported that nanosheets are formed at lower temperatures (e.g., 60–100 °C), nanotubes are formed at 100–180 °C, while nanowires are obtained at higher temperature (e.g., $T>180$ °C) [19,29,30]. Therefore, it seems that the effect of alkaline concentration on the formation of the hydrothermal products is similar to that of the temperature. Recently, we demonstrated that the successive nanosheets, nanotubes and nanowires are three unavoidable kinetic products of the reaction of TiO_2 with NaOH under moderate alkaline condition (e.g., $C_{NaOH}=5$–12 M), and higher temperature can only accelerate the kinetic reaction rate, but cannot determine the morphologies of the products [31].

The effect of the concentration of NaOH on the formation of various titanate nanostructures was further investigated by experiments carried out at 180 °C by treating TiO_2 in NaOH solution with different concentration for different duration. SEM images of the products synthesized at 180 °C in 12 and 8 M NaOH solution for different duration are shown in Fig. 3, and the corresponding XRD patterns are shown in Fig. 4. At the beginning of the reaction of TiO_2 with 12 M NaOH solution ($t=2$ h), the product is titanate nanosheets (Fig. 3a). Nanotubes are obtained by increasing the treatment duration to 4 h (Fig. 3b). It is found that part of the nanotubes had been transformed into nanowires at the duration of 6 h (Fig. 3c). By increasing the duration to 12 h, only nanowires with lengths of several tens of micrometers and widths varying from 30 to 300 nm can be observed (Fig. 3d). Similar formation process is observed when the concentration of NaOH was set as 8 M, as shown in Fig. 3e–g. SEM observation shows that pure nanotubes are formed at $t=12$ h (Fig. 3e), and both nanotubes and nanowires are obtained by increasing the duration to 40 h. The product is nanowires after 80 h of hydrothermal treatment. XRD analysis (Fig. 4) shows that the structures

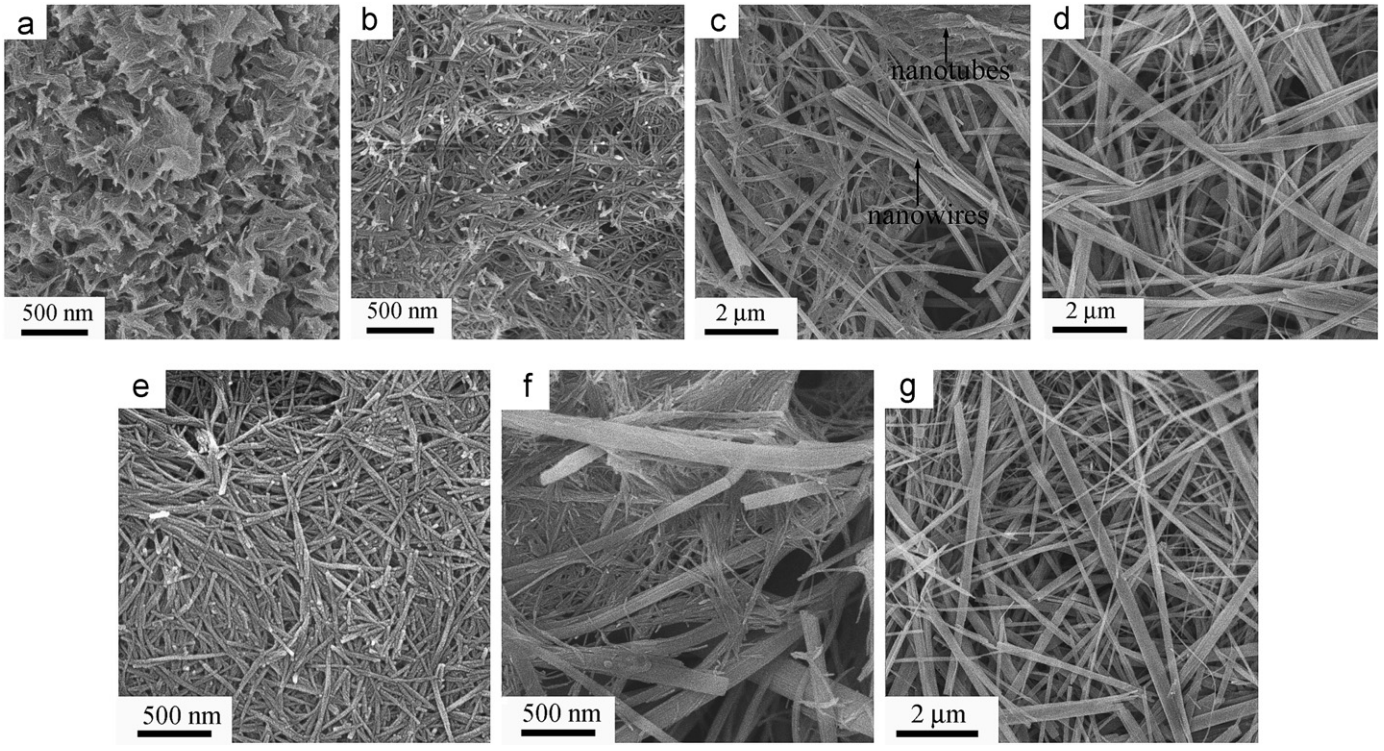

Fig. 3. SEM images of the products synthesized hydrothermally in 12 M NaOH solution at 180 °C for 2 h (a), 4 h (b), 6 h (c) and 12 h (d), and in 8 M NaOH solution for 12 h (e), 40 h (f) and 80 h (g).

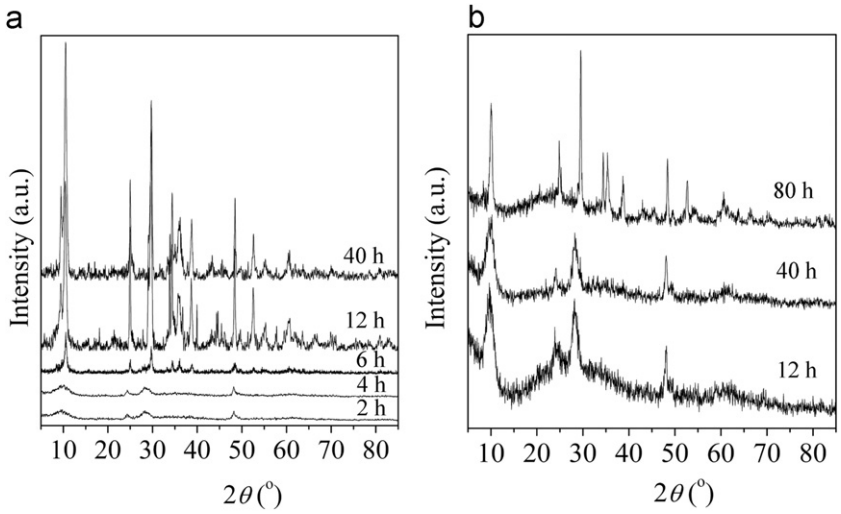

Fig. 4. XRD pattern of the hydrothermal products obtained by treating TiO_2 in 12 M (a) and 8 M (b) NaOH solution for different duration.

of both nanosheets and nanotubes can be identified as $Na_2Ti_2O_5 \cdot H_2O$, while the crystal structure of nanowires is in agreement with $NaTi_2O_4(OH)$. The foregoing morphologies observations indicate the reaction can be accelerated by increasing alkaline concentration, as shown in Figs. 1 and 3.

During the hydrothermal treatment, the reaction of precursor titania material with NaOH results in the release of titanium, as Ti(IV), probably in the form $Ti_xO_{2x+1}^{2-}$ (e.g. $Ti_2O_5^{2-}$ or $Ti_2O_4(OH)_2^{2-}$, as proposed above). The dissolved Ti(IV) nucleates and grows into lamellar titanate ($Na_2Ti_2O_5 \cdot H_2O$ nanosheets). The continuous dissolution of titania provides sufficient dissolved Ti(IV) and thus the nanosheets grows. The nanosheets will bend and scroll into nanotubes after these nanosheets reach a certain size, because of mechanical tensions [32] or asymmetrical chemical environment [33]. With further hydrothermal treatment, the nanotubes will transform into nanowires, accompanied by structure transition from $Na_2Ti_2O_5 \cdot H_2O$ to $NaTi_2O_4(OH)$. The overall hydrothermal reactions can be explained as follows:

$$2TiO_2(s)+2OH^- \rightarrow Ti_2O_5^{2-}+H_2O \quad (1a)$$

$$2Na^+ + Ti_2O_5^{2-} + H_2O \leftrightarrow Na_2Ti_2O_4(OH)_2 \text{ (i.e., } Na_2Ti_2O_5 \cdot H_2O) \quad (1b)$$

$$Na_2Ti_2O_4(OH)_2 \rightarrow NaTi_2O_4(OH)+NaOH \quad (1c)$$

where the first step (1a) represents the dissolution of titania precursor, and the second step (1b) is the crystallization of dissolved Ti(IV) from solution into solid titanate nanosheets and thereafter nanotubes, and the third step (1c) corresponds to the transformation of nanotubes into nanowires. Besides the crystallization of dissolved Ti(IV) into titanate nanosheets, the dissolved Ti(IV) that exists in the inner channel of nanotubes may recrystallize there, which helps to the transformation from nanotubes to nanowires. Thereby, the reaction rate and the morphologies of the products should be related to the concentration of dissolved Ti(IV). Fig. 5 shows the concentration of dissolved Ti(IV) ($C_{Ti(IV)}$) as a function of the concentration of NaOH. It is obvious that $C_{Ti(IV)}$ increased with C_{NaOH} and can be approximated by a linear fit of the data to the following expression:

$$\ln(C_{Ti(IV)}) = -12.25 + 0.33C_{NaOH} \quad (2)$$

The formation rate of nanosheets, nanotubes and nanowires is controlled by the rate of diffusion, while the diffusion depends on the concentration of dissolved Ti(IV). The increase of alkaline concentration leads to faster dissolution of TiO_2 and higher

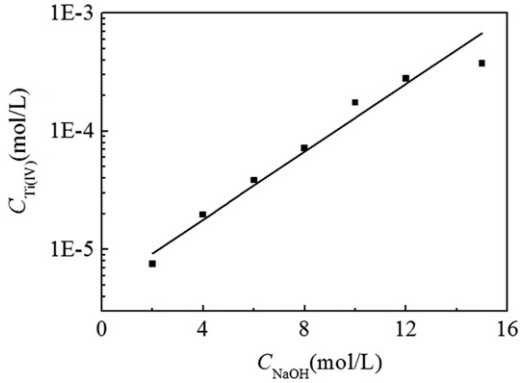

Fig. 5. The concentration of dissolved Ti(IV) as a function of the concentration of NaOH solution. The reaction temperature is 180 °C and the duration is 24 h.

concentration of dissolved Ti(IV), which means an improved mass transfer capability in the reaction system. As a result, the reaction was accelerated.

We demonstrated that the reaction rate for the formation of both nanotubes and nanowires can be accelerated by increasing alkaline concentration. However, it is surprising that the product is amorphous titanate if C_{NaOH} was further increased to 15 M, as shown in Fig. 1e. ICP detection indicates that the mole Ti/Na ratio is 1.06 for the amorphous titanate, which is similar to that of titanate nanosheets (Ti/Na = 1.05) and nanotubes (Ti/Na = 0.97). Thermogravimetric analysis (TGA) study suggests that the chemical composition of the protonated amorphous titanate can be described as $H_2Ti_{2.27}O_{5.54} \cdot 2.2H_2O$. Therefore, based on the ICP and TGA observations, the chemical composition of the amorphous sample is proposed as $Na_2Ti_2O_5 \cdot nH_2O$. Further study shows that the product should be amorphous particles if C_{NaOH} is extremely high. Fig. 6 shows several typical TEM images of the hydrothermal products obtained by treating TiO_2 in 20 M NaOH solution at different temperature for different durations. All of the products are amorphous particles. It is obvious that the formation of amorphous particles is determined only by the concentration of NaOH, but independent on the temperature or duration. It is noticed that the concentration of dissolved Ti(IV) is related to the concentration of NaOH, higher C_{NaOH} means higher $C_{Ti(IV)}$. As shown in Fig. 5, the concentration of dissolved Ti(IV) is increased from 7.52×10^{-6} to 3.75×10^{-4} M while the concentration of NaOH increases from 2 to 15 M. Sugimoto and Kojima [34–36]

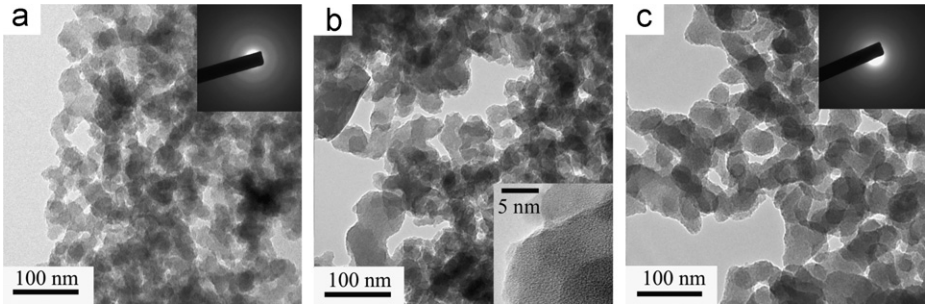

Fig. 6. TEM images of the hydrothermal products obtained by treating TiO_2 in 20 M NaOH solution at different temperature for different durations: (a) 120 °C, 8 h, (b) 150 °C, 144 h and (c) 210 °C, 144 h. Insets are SAED patterns (a and c) and HRTEM image (b).

studied the solubility of $Ti(OH)_4$ gel in different solvents at room temperature. They found that the yield of TiO_2 precipitation was lowered from 100% to 2.1% when the solubility of the $Ti(OH)_4$ gel was increased from about 10^{-6} to 1.34×10^{-4} M.

The reason for the formation of amorphous titanate is proposed as follows. Under condition of higher NaOH concentration, the dissolution of titania precursor results in abundant dissolved Ti(IV) (formula 1a). At the same time, the alkaline solution is very viscous if the NaOH concentration is extremely high, and the diffusion of Ti(IV) ion is thus restricted. Additionally, it is found that not only titania, but also titanate nanotubes/nanowires were decomposed into amorphous titanate particles when they were treated with ultra-high concentrated NaOH solution ($C_{NaOH}>15$ M) [37], which suggests that crystallized titanate are unstable in the extreme concentrated alkaline solution, and the decomposition rate of crystal titanate should be very fast. It is thus believed that the crystallization of the dissolved Ti(IV) from solution into solid titanate is prevented, while the dissolution of solid titanate is encouraged, due to the high solubility of Ti(IV) (formula 1b) and the depressed mass transfer capability. As a result, a great deal of Ti(IV) ion, instead of solid titanate crystals, exists in the viscous solution during the hydrothermal treatment. In this case, the nucleation density should be very high, and the diffusion of the atoms is hindered. Accordingly, the formation of amorphous particles is encouraged.

The evolution of the products was also found to disobey the proposed "TiO_2 precursor→nanosheets→nanotubes→nanowires" transformation mechanism [31], if the concentration of NaOH was decreased to a low value, such as 4 M. Fig. 7 depicts the morphologies evolution of the hydrothermal products obtained by treating TiO_2 in 4 M NaOH solution at 180 °C for different durations. After 24 h of hydrothermal treatment, most of the TiO_2 precursor has transformed into titanate nanosheets, as shown in Fig. 7a. The nanosheets show typical thickness of about 6 nm, width of about 12–20 nm and lengths of several hundred nanometers. These nanosheets grow as the reaction duration increased. As the duration is increased to 96 h, the nanosheets have thickness of about 8–15 nm, width of about 20–40 nm and length of about several micrometers, as shown in Fig. 7b. By increasing the duration to 160 h, a considerable amount of nanowires with width of about 60–90 nm and length of several and even several tens of micrometers were found together with smaller nanosheets, as shown in Fig. 7c. Most of the nanosheets have transformed into nanowires after 240 h of hydrothermal treatment (Fig. 7d). It is noticed that no nanotube was detected during the overall reaction process.

Fig. 8 shows the pore volume distribution (BJH desorption) of the nanotubes (see Fig. 3e) and the mixture of nanowires and nanosheets (see Fig. 7c). The nanotubes exhibit a sharp pore size distribution with a maximum peak of 3.8 nm, which correspond to the pores inside the nanotubes and thus this diameter is equal to the inner diameter of the nanotubes. However, the mixture of nanowires and nanosheets only shows a broad peak around 20 nm (8–60 nm). The disappearance of the smaller pores (about 4 nm) indicates that both nanowires and nanosheets are not hollow, and suggests that no nanotubes can be formed during the hydrothermal treatment of TiO_2 with 4 M NaOH solution.

Based on the SEM and BJH observation, it is deduced that titanate nanosheets can transform into nanowires directly, without the presence of nanotubes as intermediate. So far, most of the reported syntheses were performed in the condition of moderate NaOH solution, typically, $C_{NaOH}=10$ M. Accordingly, nanotubes were formed before the appearance of nanowires. The successive nanosheets, nanotubes and nanowires should be the three unavoidable kinetic products of the reaction of TiO_2 with NaOH under moderate alkaline condition (see schematic Fig. 9). However, no nanotube was formed under low alkaline condition. It is believed that the different evolution route of titanate products under different alkaline conditions is controlled by the NaOH concentration. As mentioned above, for the nanosheets obtained under moderate NaOH solution, they have width of about 20–30 nm and thickness less than 4 nm before scrolling into nanotubes. However, for nanosheets obtained under low concentration of NaOH, they show typical thickness of about 6 nm when their width is only 12–20 nm. It is thus proposed that with the decrease of alkaline concentration, the thickness of the nanosheets grows faster, compared with the growth rate along the width of nanosheets; the decrease in alkaline concentration may also result in a slower rate of nanosheets scrolling. In this case, the nanosheet is too rigid to bend before curving occurs. As a result, nanowires instead of nanotubes were formed by the thickening of nanosheets. A schematic drawing depicting the evolution of the hydrothermal products under different alkaline condition is shown in Fig. 9.

3.2. *Application of titanate nanostructures for wastewater treatment*

Titanate nanotubes have been the focus of numerous investigations for promising applications as adsorbents and photocatalysts for the removal of metal ions and dyes from water system [9,23,24,38–41], as they offer a larger surface area, flexible interlayer distances, and high cation exchange capacity and also provide channels for enhanced electron transfer [24,42]. Herein, the adsorption and photocatalysis behaviors of these three different hydrothermal products (nanotubes, nanowires and amorphous nanoparticles) were studied. Firstly, the cation exchange behavior of the above-mentioned titanates was comparatively studied. Pb^{2+} obtained from the nitrate salt was selected as the first adsorbate in order to examine the toxic metal ions removal capacities of these three titanate products, as shown in Fig. 10. The saturation capacities of the titanate nanotubes,

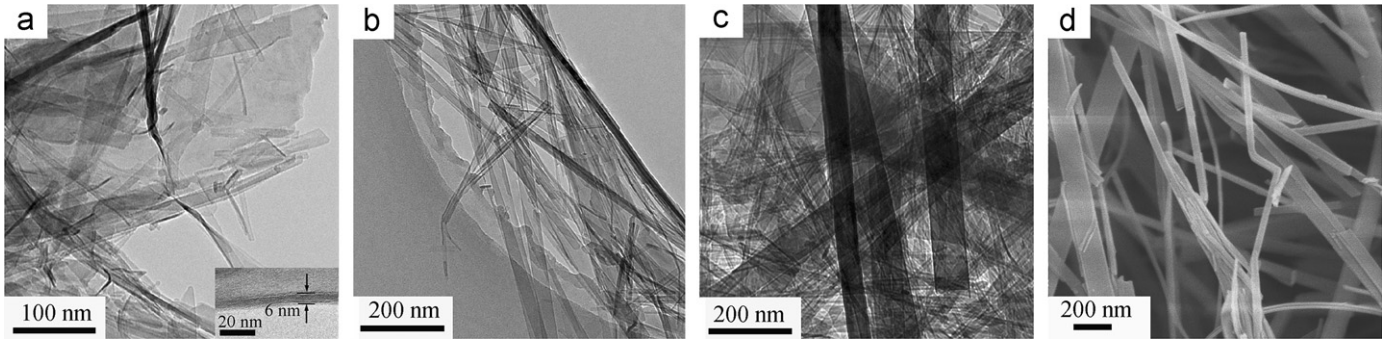

Fig. 7. TEM images (a–c) and SEM image (d) of the hydrothermal products obtained by treating TiO_2 in 4 M NaOH solution at 180 °C for (a) 24 h, (b) 96 h, (c) 160 h and (d) 240 h.

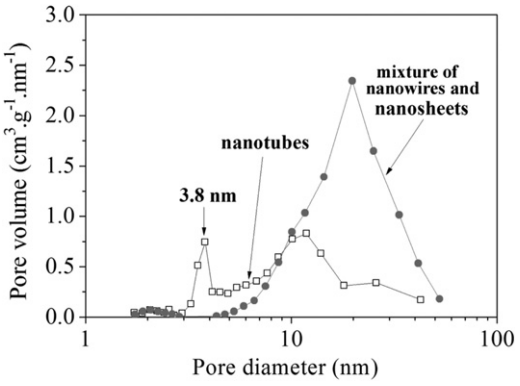

Fig. 8. Pore volume distribution (BJH desorption) of the nanotubes (see Fig. 3e) and the mixture of nanowires and nanosheets (see Fig. 7c).

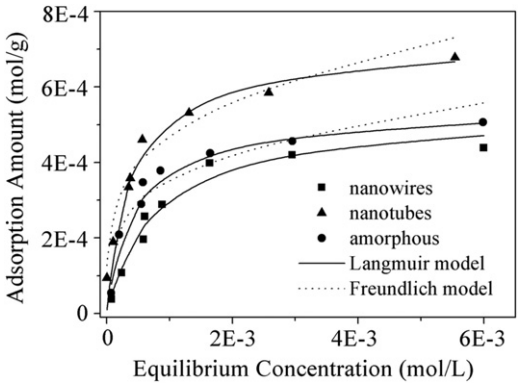

Fig. 10. The adsorption isotherms of Pb^{2+} on protonated titanate nanotubes, nanowires and amorphous titanate nanoparticles.

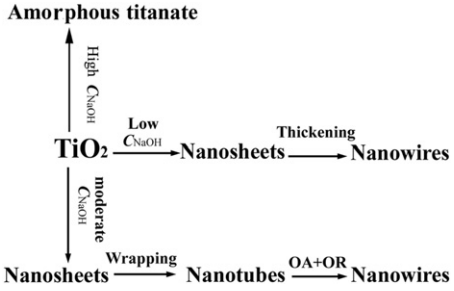

Fig. 9. Schematic of the formation of different titanate nanostructures under different NaOH concentration.

nanowires and amorphous titanate nanoparticles are 0.71, 0.51 and 0.54 mmol/g, respectively. In order to obtain insight into the possible mechanisms for removing Pb^{2+} ions from aqueous solution onto different titanate adsorbents, the adsorption equilibrium data were analyzed using Langmuir and Freundlich models [43,44].

$$Q_e = \frac{C_e Q_m K_L}{1 + C_e K_L} \tag{3a}$$

$$Q_e = K_F C_e^{1/n} \tag{3b}$$

where C_e is the equilibrium metal ions concentration in solution (mol/L), Q_e is the amount of adsorbed ions (mol/g), Q_m is the maximum adsorption capacity (mol/g), K_L (L/mol) is the Langmuir constant, and K_F (mol/g(L/mol)$^{1/n}$) and n are the Freundlich constants. The fitting results of both Langmuir and Freundlich models are shown in Fig. 10. Generally, the adsorption environment may be heterogeneous if the adsorption causes a serious disorder in the structure of the titanate. However, as shown in Fig. 10, it is obvious that Langmuir model is in good agreement with the experimental data, while Freundlich model does not give a good fit. The fitting results indicate that the adsorption environment in these titanates can be viewed as homogeneous system.

The photocatalytic activities of these three titanate nanostructures were studied by the photodegradation of methylene blue in aqueous solution. Fig. 11a shows the photocatalytic curves of the protonated titanate nanotubes, nanowires and amorphous titanate nanoparticles. Obviously, the activity of nanotubes is much higher than that of nanowires (and amorphous nanoparticles). About 71% of the dye is degraded by nanotubes after irradiation for 3 h. In addition, from the plots of $\ln(C_0/C)$ versus irradiation time in Fig. 11b, it is found that the photocatalytic degradation accords with first-order kinetics, i.e., $\ln(C_0/C)=kt$. Via the first-order linear fit, the determined reaction constant k was 0.0075, 0.0031 and 0.0011 min^{-1} for the protonated titanate nanotubes, nanowires and amorphous nanoparticles, respectively. It is obvious that the k value of nanotubes is the largest, about 13 times higher than that of amorphous nanoparticles. Generally, the photocatalytic activity of the photocatalyst depends on its particle size, surface area, defect chemistry and adsorbability [45]. Apparently, a higher surface area can offer more active adsorption sites and photocatalytic reaction centers, and smaller particles are usually advantageous for photocatalysis due to the reduction of volume charge–carrier recombination. Additionally, adsorption of dye onto the photocatalyst is also an important factor affecting the degradation, because the dye molecules have to be adsorbed on the surface of photocatalyst particles first before being decomposed. The BET surface area is about 230 m^2/g for nanotubes, 30 m^2/g for nanowires and 400 m^2/g for amorphous nanoparticles. The saturation adsorbabilities of nanotubes, nanowires and amorphous nanoparticles are 0.25, 0.017 and 0.011 mmol/g,

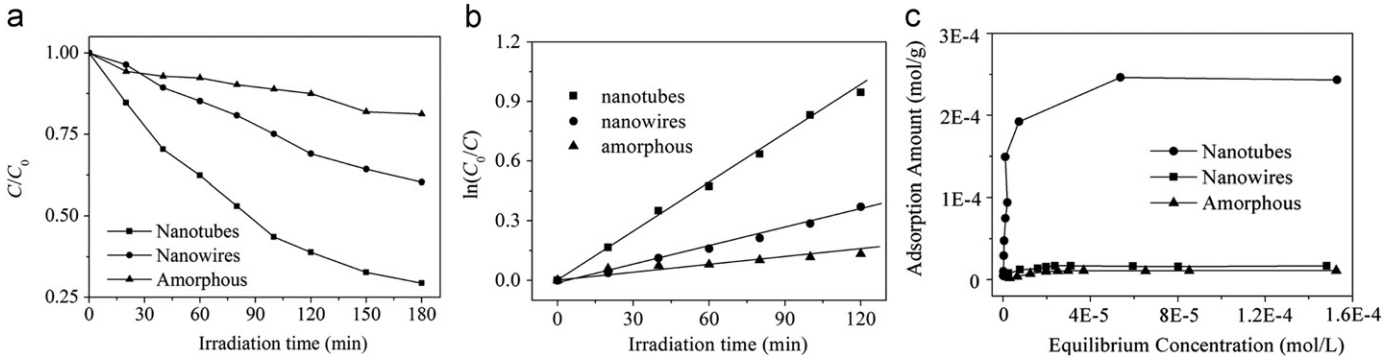

Fig. 11. (a) The photocatalytic activities of the protonated titanate nanotubes, nanowires and amorphous nanoparticles for the degradation of methylene blue, (b) first-order plots for the photocatalytic degradation and (c) adsorption isotherms of dye onto the titanate adsorbents.

respectively (see Fig. 11c). Obviously, the nanotubes possess large surface area and high adsorption capacity. Consequently, the photocatalytic activity of nanotubes is far higher than that of nanowires/amorphous nanoparticles. Though the surface area of nanowires is far lower than that of amorphous nanoparticles, the photocatalytic activity of nanowires is still higher than that of the amorphous nanoparticles. The higher photocatalytic activity of nanowires might be due to the enhancement of the crystallization.

4. Conclusion

In summary, we report the effect of the concentration of NaOH on the formation and transformation of various titanate nanostructures derived from the hydrothermal reaction. The varying of NaOH concentration leads to three distinct formation mechanisms. The reaction of TiO_2 with NaOH yields dissolved Ti(IV), and the concentration of Ti(IV) increases with increase in NaOH concentration. Under the moderate NaOH condition (C_{NaOH}= 5–12 M), the Ti(IV) nucleates and grows into $Na_2Ti_2O_5 \cdot H_2O$ nanosheets. After that, the nanosheet grows and then scrolls into orthorhombic $Na_2Ti_2O_5 \cdot H_2O$ nanotube. The nanotubes should transform into monoclinic $NaTi_2O_4(OH)$ nanowires as the hydrothermal duration increases. The formation of these titanate nanostructures is accelerated by increasing NaOH concentration. However, further increases of the concentration of NaOH ($C_{NaOH} > 15$ M) results in the formation of amorphous titanate, due to the increased concentration of dissolved Ti(IV) and decreased mass transfer capability. On the other hand, under the low NaOH condition ($C_{NaOH} < 5$ M), the crystallization rate along the width of the nanosheet is depressed compared to that along the thickness direction. The nanosheet is far thicker than that obtained in moderate NaOH solution, and it is too rigid to bend. Consequently, no nanotubes can be formed, and nanowires are obtained directly by the thickening of nanosheets. Furthermore, adsorption and photocatalysis studies show that the three different hydrothermal products (nanowires, amorphous nanoparticles and especially nanotubes) might be potential adsorbents for the removal of both heavy metal ions and dyes and photocatalysts for the removal of dyes from wastewater.

Acknowledgments

This work was supported by the National Natural Science Foundation of China (20901079), the National Basic Research Program (2007CB936700), and the Key Program of Science and Technology in Fujian Province (2009H0045, 2009I0028).

References

[1] T. Kasuga, M. Hiramatsu, A. Hoson, T. Sekino, K. Niihara, Langmuir 14 (1998) 3160.
[2] B. Zhang, F. Chen, W.W. Qu, J.L. Zhang, J. Solid State Chem. 182 (2009) 2225.
[3] D.V. Bavykin, F.C. Walsh, Eur. J. Inorg. Chem. (2009) 977.
[4] B.X. Wang, Y. Shi, D.F. Xue, J. Solid State Chem. 180 (2007) 1038.
[5] B.C. Viana, O.P. Ferreira, A.G.S. Filho, J.M. Filho, O.L. Alves, J. Braz. Chem. Soc. 20 (2009) 167.
[6] X.B. Chen, S.S. Mao, Chem. Rev. 107 (2007) 2891.
[7] H.Y. Zhu, Y. Lan, X.P. Gao, S.P. Ringer, Z.F. Zheng, D.Y. Song, J.C. Zhao, J. Am. Chem. Soc. 127 (2005) 6730.
[8] C.Y. Xu, Q. Zhang, H. Zhang, L. Zhen, J. Tang, L.C. Qin, J. Am. Chem. Soc. 127 (2005) 11584.
[9] D.J. Yang, Z.F. Zheng, H.Y. Zhu, H.W. Liu, X.P. Gao, Adv. Mater. 20 (2008) 2777.
[10] A. Riss, T. Berger, S. Stankic, J. Bernardi, E. Knozinger, O. Diwald, Angew. Chem. Int. Ed. 47 (2008) 1496.
[11] J.Q. Huang, Z. Huang, W. Guo, M.L. Wang, Y.G. Cao, M.C. Hong, Cryst. Growth Des. 8 (2008) 2444.
[12] L. Torrente-Murciano, A.A. Lapkin, D.V. Bavykin, F.C. Walsh, K. Wilson, J. Catal. 245 (2007) 272.
[13] D.V. Bavykin, A.A. Lapkin, P.K. Plucinski, J.M. Friedrich, F.C. Walsh, J. Phys. Chem. B 19 (2005) 19422.
[14] S.H. Lim, J. Luo, Z. Zhong, W. Ji, J. Lin, Inorg. Chem. 44 (2005) 4124.
[15] G.S. Kim, H.K. Seo, V.P. Godble, Y.S. Kim, O.B. Yang, H.S. Shin, Electrochem. Commun. 8 (2006) 961.
[16] E. Enache-Pommer, J.E. Boercker, E.S. Aydil, Appl. Phys. Lett. 91 (2007) 123116.
[17] J.R. Li, Z.L. Tang, Z.T. Zhang, Chem. Mater. 17 (2005) 5848.
[18] H. Zhang, X.P. Gao, G.R. Li, T.Y. Yan, H.Y. Zhu, Electrochim. Acta 53 (2008) 7061.
[19] Y. Lan, X.P. Gao, H.Y. Zhu, Z.F. Zheng, T.Y. Yan, F. Wu, S.P. Ringer, D.Y. Song, Adv. Funct. Mater. 15 (2005) 1310.
[20] H. Tokudome, M. Miyauchi, Angew. Chem. Int. Ed. 44 (2005) 1974.
[21] C.H. Han, D.W. Hong, I.J. Kim, J. Gwak, S.D. Han, K.C. Singh, Sensors Actuators B 128 (2007) 320.
[22] D.V. Bavykin, J.M. Friedrich, F.C. Walsh, Adv. Mater. 18 (2006) 2807.
[23] X.M. Sun, Y.D. Li, Chem. Eur. J. 9 (2003) 2229.
[24] C.K. Lee, S.S. Liu, L.C. Juang, C.C. Wang, M.D. Lyu, S.H. Hung, J. Hazard. Mater. 148 (2007) 756.
[25] D.L. Morgan, H.W. Liu, R.L. Frost, E.R. Waclawik, J. Phys. Chem. C 114 (2010) 101.
[26] C.C. Tsai, H.S. Teng, Chem. Mater. 18 (2006) 367.
[27] J.J. Yang, Z.S. Jin, X.D. Wang, W. Li, J.W. Zhang, S.L. Zhang, X.Y. Guo, Z.J. Zhang, Dalton Trans. (2003) 3898.
[28] C.W. Peng, M. Richard-Plouet, T.Y. Ke, C.Y. Lee, H.T. Chiu, C. Marhic, E. Puzenat, F. Lemoigno, L. Brohan, Chem. Mater. 20 (2008) 7228.
[29] E. Horvath, A. Kukovecz, Z. Konya, I. Kiricsi, Chem. Mater. 19 (2007) 927.
[30] Z.Y. Yuan, B.L. Su, Colloid. Surf. A-Physicochem. Eng. Asp. 241 (2004) 173.
[31] J.Q. Huang, Y.G. Cao, Q.F. Huang, H. He, Y. Liu, W. Guo, M.C. Hong, Cryst. Growth Des. 9 (2009) 3632.
[32] D.V. Bavykin, V.N. Parmon, A.A. Lapkin, F.C. Walsh, J. Mater. Chem. 14 (2004) 3370.
[33] S. Zhang, L.M. Peng, Q. Chen, G.H. Du, G. Dawson, W.Z. Zhou, Phys. Rev. Lett. 91 (2003) 256103.
[34] T. Sugimoto, T. Kojima, J. Phys. Chem. C 112 (2008) 18760.
[35] T. Sugimoto, T. Kojima, J. Phys. Chem. C 112 (2008) 18437.
[36] T. Sugimoto, T. Kojima, J. Phys. Chem. C 112 (2008) 18445.
[37] J.Q. Huang, Y.G. Cao, M.L. Wang, C.G. Huang, Z.H. Deng, H. Tong, Z.G. Liu, J. Phys. Chem. C 114 (2010) 14748.
[38] H. Kochkar, A. Turki, L. Bergaoui, G. Berhault, A. Ghorbel, J. Colloid Interface Sci. 331 (2009) 27.
[39] C.K. Lee, C.C. Wang, M.D. Lyu, L.C. Juang, S.S. Liu, S.H. Hung, J. Colloid Interface Sci. 316 (2007) 562.

[40] L. Shang, B.J. Li, W.J. Dong, B.Y. Chen, C.R. Li, W.H. Tang, G. Wang, J. Wu, Y.B. Ying, J. Hazard. Mater. 178 (2010) 1109.
[41] S. Chatterjee, K. Bhattacharyya, P. Ayyub, A.K. Tyagi, J. Phys. Chem. C 114 (2010) 9424.
[42] M. Grandcolas, A. Louvet, N. Keller, V. Keller, Angew. Chem. Int. Ed. 48 (2009) 161.
[43] S. Debnath, U.C. Ghosh, Chem. Eng. J. 152 (2009) 480.
[44] S.S. Liu, C.K. Lee, H.C. Chen, C.C. Wang, L.C. Juang, Chem. Eng. J. 147 (2009) 188.
[45] X. Wei, G. Xu, Z.H. Ren, C.X. Xu, G. Shen, G.R. Han, J. Am. Ceram. Soc. 91 (2008) 3795.